Journal of Metals, Materials and Minerals, 34(3), 1968, 2024

ZnO nanostructures synthesized by one-step sol-gel process using different zinc precursors

Maneerat SONGPANIT[1], Kanokthip BOONYARATTANAKALIN[1], Wisanu PECHARAPA[1], and Wanichaya MEKPRASART[1,*]

[1] *College of Materials Innovation and Technology, King Mongkut's Institute of Technology Ladkrabang, Bangkok, 10520, Thailand*

***Corresponding author e-mail**: wanichaya.me@kmitl.ac.th

Received date:
18 February 2024
Revised date:
30 June 2024
Accepted date:
30 June 2024

Keywords:
ZnO nanostructures;
Sol-gel process;
Zinc precursors

Abstract

Zinc oxide (ZnO) nanopowders have been widely applied in electronics, optics and photocatalytic applications depending on their morphological structure. In the bottom-up process, it is conceived that the different zinc precursors may result in different formations of ZnO nanostructures with exceptional morphology. This work focuses on ZnO material synthesized via the facile sol-gel synthesis using different zinc slat precursors, including zinc acetate, zinc nitrate, zinc sulphate, and zinc chloride. All zinc salt precursors were incorporated with sodium hydroxide and hexamethylenetetramine (HMTA) under mild thermal energy with consistent conditions to investigate ZnO formation. The as-prepared samples appeared in white powders with different aggregation features. The crystalline phase, surface morphologies, and element mapping of all ZnO samples were analyzed using X-ray diffraction technique (XRD) and field emission scanning electron microscope (FE-SEM). The chemical bonding structure of ZnO powders was characterized by Fourier transform infrared spectroscopy (FTIR) and Raman spectroscopy. The specific surface area per volume of ZnO nanopowders obtained by different zinc salt precursors was analyzed by Brunauer-Emmett-Teller (BET) method. All ZnO samples obtained from various zinc salt precursors exhibited a high crystallinity of the wurtzite structure without other impurities. The structural properties of ZnO nanopowders demonstrated different sizes and structures with distinguished formation and aggregation depending on the zinc precursor basic strength being used.

1. Introduction

Recently, the interest in complex metal oxides as a type of semiconductor has rapidly increased due to their suitability and unique biological, optical, physical, and chemical properties [1], offering potential applications as evident properties in nanoscale [2]. There is a prevalent trend in synthesizing materials with nanoscale structures for diverse applications, growing in popularity across various industries. This popularity is attributed to the confined physical dimensions of nanomaterials, typically ranging from 1 nm to 100 nm [3]. The movement of electrons within nanomaterials differs significantly from that in ordinary bulk materials due to their high surface area to volume ratio, leading to the appearance of unique physical and chemical properties. This phenomenon is particularly evident in nanoscale metal oxide materials, such as zinc oxide (ZnO) [4] and titanium dioxide (TiO_2) [5], widely used across various industries. Zinc oxide is an attractive semiconductor material owing to its numerous benefits, widespread applications, and environmentally friendly [6]. The prominent properties of zinc oxide have been utilized as optical devices with high transparency in the near-UV region [7], an excellent candidate for photoconductive materials [8], its preferable tetrahedral structure for the piezoelectric material [9], its high aspect ratio for sensitive gas-sensing characteristics [10], and significant active on antibacterial activity [11]. The notable electrical, optical, and environmental properties of ZnO material are currently of great interest, particularly in nanomaterials. Meanwhile, zinc oxide can exhibit appreciable photocatalytic activity in organic chemical dye degradation [12]. Due to its characteristics as a n-type semiconductor with a wide band gap energy at 3.37 eV [13], light-accelerated reactions or high energy activation are required for the generation of electron-hole pairs in ZnO material. Thus, the development of ZnO photocatalyst utilizing the piezoelectric effect has recently become attractive in wastewater treatment. ZnO is one of the dominant piezoelectric materials because of its high effective piezoelectric coefficient d33, especially in ZnO nanorods at 130 $pm \cdot V^{-1}$ [14]. Therefore, the design of ZnO morphologies in nanoscale-based catalysts plays a key role in possessing photogenerated electron-hole pairs with a high active surface area, which contributes to the suppression of charge recombination and energy loss, ultimately leading to excellent photocatalytic activities [15].

Several methods for ZnO material synthesis have been proposed, such as chemical vapor condensation [16], arc discharge [17], micro-emulsion [18], hydrothermal [19], precipitation [20], sonochemical reaction [21], and sol-gel method [22]. All processes typically offer to produce ZnO material with low-dimensional structures often involving substantial quantities of chemicals, resulting in increased waste production. Meanwhile, low-dimensional ZnO structures through a simple chemical method are highly intriguing. The one-step sol-gel method without calcination is effective for crafting nano- or micro-sized rods or sheet-like structures. This method effectively amplifies the surface area and harnesses the exceptional material properties for sensing and photocatalytic applications [23]. In addition, the various morphologies of ZnO structures are categorized based on their dimensional characteristics, which contribute to the prominent properties, particularly at the nanoscale. One-dimensional (1D) ZnO materials exhibit nanoscale morphologies, including nanorods, nanowires, and nanotubes, which are among the most significant materials owing to their attractive physical characteristics, particularly enhanced piezoelectric properties and energy harvesting capabilities [24]. Secondly, two-dimensional structures of ZnO are demonstrated in coating forms, for example, nano-coatings, nano-films, and nano-layers. Low resistivity, high electron mobility, and large optical band gaps of uniform ZnO thin film can be achieved by a 2D structured arrangement of a flower-like layer on the substrate [25]. The last category is three-dimensional (3D) ZnO material, which is not confined to the nanoscale and is included in bulk powder-like nanoparticles, bundles of nanowires, and multi-nanolayers [26]. The hierarchical structures of 3D-ZnO typically provide high surface-to-volume ratios, a large accessible surface area, and enhanced permeability. Additionally, the hierarchical ZnO structures can improve light traveling paths and facilitate light absorption, which is beneficial for the fabrication of functional devices including sensors and photocatalysts [27]. The distinction among ZnO structures significantly impacts their properties, extensively explored for various applications, especially in nanorod structures. ZnO nanorods, characterized by exclusive optical and electronic properties, are particularly popular due to their precise directional length, making them suitable for growth-oriented applications, for example, sensing membranes, energy storages, light-emitting diodes, and piezoelectric devices. Moreover, ZnO nanorods can aggregate to form new structures such as nano-flowers or nano-flakes [28], enhancing surface area and benefiting applications such as photocatalytic degradation.

This research aims to synthesize ZnO nanopowders using various zinc salt precursors, including zinc acetate, zinc nitrate, zinc sulphate, and zinc chloride, by a one-step sol-gel process without a post-treatment step. However, the impact of these diverse zinc precursors on the physical properties of the ZnO material obtained via a low operating temperature under consistent conditions, including a constant precursor molar ratio, the same reaction temperature, and a steady HMTA content in each experiment has seldom been explored. Consequently, the formation and reaction of ZnO are predominantly proposed and investigated using different zinc salt precursors. The morphology, structural properties, and chemical bonding of ZnO samples demonstrated different sizes and flake-like structures with distinguished formation and aggregation depending on the zinc precursor being used.

2. Experimental

ZnO nanopowders were synthesized by one-step sol-gel process with various zinc starting materials of zinc acetate, zinc nitrate, zinc sulfate, and zinc chloride. Each zinc salt precursor at 20 mmol was dissolved in 50 mL of deionized (DI) water using an ultrasonic bath for 15 min. The concentration of hexamethylenetetramine (HMTA) at 2.3 mmol was added to the zinc precursor solution and subjected to continuous ultrasonication at room temperature for 15 min. 2 M of sodium hydroxide (NaOH) solution was prepared by dissolving 50 mL DI water under ultrasonication for 15 min to form a white slurry. Subsequently, the zinc precursor solution with HMTA and NaOH solution was mixed using an ultrasonic bath for 15 min. The mixture of different zinc salt precursors was then allowed to stand at 80°C for 24 h. Afterward, ZnO products with various starting materials were separated by centrifugation at 2,500 rpm for 20 min. The precipitates were washed with DI water and ethanol until pH 7. Finally, the products of all samples were dried overnight at 60°C. The as-prepared samples appeared as white powders with varying aggregation features. The structural phases, surface morphologies, and element mapping of the ZnO products were characterized using X-ray diffraction (XRD; Rigaku SmartLab) and field emission scanning electron microscopy (FE-SEM; JSM-7001F and Hitachi S-8030). The chemical bonding structures of ZnO powders were characterized by Fourier transform infrared spectroscopy (FT-IR; PerkinElmer) and Raman spectroscopy (Raman; Renishaw inVia Raman microscope). Additionally, the specific surface area per unit volume of the various ZnO structures was analyzed using the Brunauer-Emmett-Teller (BET) method with a Quantachrome Autosorb iQ-C-XR-XR-XR instrument.

3. Results and discussion

During the synthesis, all zinc salt precursors were completely dissolved in water. HMTA solution was added in the heated solution causing the formation of a milky solution. The production of hydroxide ions (OH^-) from HMTA hydrolysis under thermal conditions yields Zn hydroxide intermediate. Then the Zn hydroxide dehydration produces ZnO product [29]. The microstructural features of ZnO products from various zinc precursors were examined using field emission scanning electron microscopy, as illustrated in Figure 1. The different zinc precursors affect the structure of ZnO nano-powders with a distinct size and a flake-like structure [30]. The diverse morphologies observed in zinc oxide products are attributed to variations in growth rates associated with distinct crystallographic planes by the influence of the zinc precursor basic strength ($Cl^- < NO_3^- < SO_4^{2-} < CH_3COO^-$). In the case of zinc acetate precursor (Figure 1(a)), ZnO nanopowder exhibited a high degree of agglomeration, forming large flake-like shapes and small rod-like in some areas due to the stronger basic solution compared to the other precursors. Conversely, ZnO materials synthesized from zinc sulphate and zinc chloride precursors, as shown in Figure 1(b-c), demonstrated plate-like structures. The ZnO powders observed less particle aggregation than those produced from the zinc acetate precursor [31]. The morphology of ZnO powder by zinc nitrate precursor in Figure 1(d) exhibited high agglomeration, forming flake-like structures, contributing to the larger area. The negligible basicity of Cl^-, NO_3^-, and SO_4^{2-} ions affect the morphology of ZnO nanostructure yield the flake-like structure. Furthermore, the elemental mapping result of Zn element from ZnO nanopowders synthesized using different zinc salt precursors is illustrated in Figure 2. A high distribution of Zn atoms on the ZnO powders was observed. The high purity of the obtained ZnO nanostructures via a facile sol-gel method under mild thermal energy could be confirmed by EDS spectra. The highest atomic percentage of Zn element, approximately 80% was consistent across all zinc precursors (the insert figures in Figure 2), indicating the purity of ZnO formation in comparison to the atomic percentages of O and other elements, as presented in Table 1.

The XRD patterns within the range of 15° to 75° of ZnO nanopowders derived from various zinc precursors are illustrated in Figure 3. The high crystallinity of all ZnO samples was related to the wurtzite structure and hexagonal lattice. No characteristic peaks of other impurities, such as NaOH precursor and salt products appear in the patterns confirming the purity of ZnO products. The evident peaks of all ZnO samples at 2θ of 31.8°, 34.4°, 36.3°, 47.6°, 56.6°, 62.9°, 66.4°, 68.0°, 69.1° and 72.6° were related to the crystalline planes of (100), (002), (101), (102), (110), (103), (200), (112), (201) and (004) (ICSD No. 167690). The formations of ZnO nanopowders using different zinc starting precursors were created by chemical reaction as following the Equation (1-4) [32].

The reaction involving zinc acetate is represented by chemical reaction (1)

$$Zn(CH_3COO)_2+2NaOH \xrightarrow[\Delta T]{\text{HMTA and } H_2O} ZnO+2CH_3COONa+H_2O \quad (1)$$

The reaction involving zinc sulphate is represented by chemical reaction (2)

$$ZnSO_4+2NaOH \xrightarrow[\Delta T]{\text{HMTA and } H_2O} ZnO+Na_2SO_4+H_2O \quad (2)$$

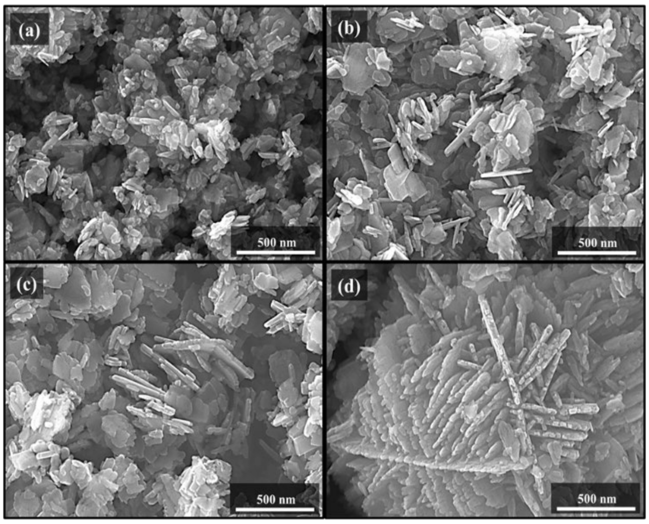

Figure 1. FE-SEM images of ZnO nanopowders with different zinc precursors of (a) zinc acetate, (b) zinc sulphate, (c) zinc chloride, and (d) zinc nitrate.

The reaction involving zinc chloride is represented by chemical reaction (3)

$$ZnCl_2+2NaOH \xrightarrow[\Delta T]{\text{HMTA and } H_2O} ZnO+2NaCl+H_2O \quad (3)$$

The reaction involving zinc nitrate is represented by chemical reaction (4)

$$Zn(NO_3)_2+2NaOH \xrightarrow[\Delta T]{\text{HMTA and } H_2O} ZnO+2NaNO_3+H_2O \quad (4)$$

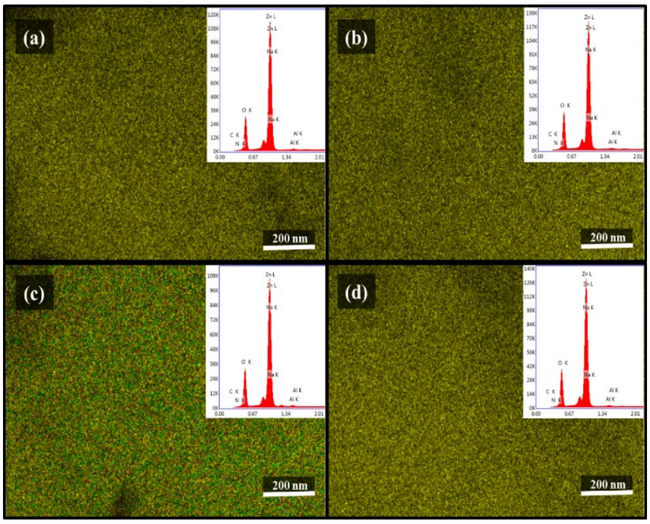

Figure 2. EDS analysis by the elemental mapping images of Zn element from ZnO nanopowders using different zinc precursors (a) zinc acetate, (b) zinc sulphate, (c) zinc chloride, and (d) zinc nitrate.

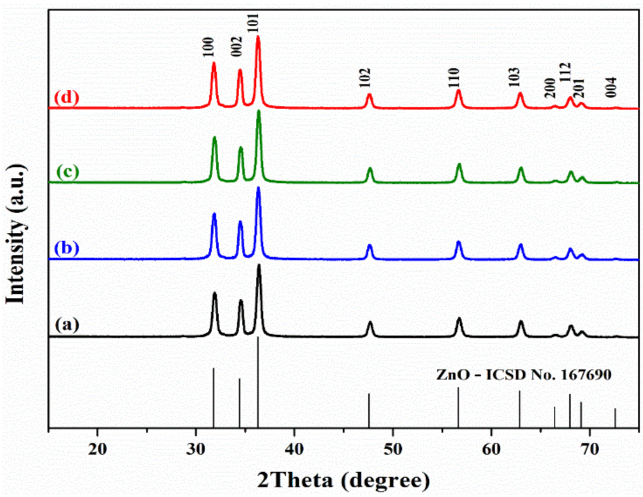

Figure 3. XRD patterns of ZnO nanopowders with different zinc precursors of (a) zinc acetate, (b) zinc sulphate, (c) zinc chloride, and (d) zinc nitrate.

Table 1 Atomic percentage by EDS technique of ZnO nanopowders synthesized by different zinc precursors.

Sample	Atomic (%)		
	Zn	**O**	**Other elements**
Zinc acetate	81.93	16.29	1.78
Zinc sulphate	79.27	17.93	2.80
Zinc chloride	81.06	16.95	1.99
Zinc nitrate	79.30	18.11	2.59

The formation of ZnO products can be attributed to the ion exchange process between Zn ions and NaOH base solution under gentle thermal energy, serving as the mechanisms for the precursor transformation. Meanwhile, the generation of anions by various zinc precursors was found to affect the diverse ZnO morphologies, as proposed in the SEM discussion. The crystalline structure of ZnO products can be completely formed through sufficient thermal energy at 80°C, leading to the decomposition of the zinc hydroxide intermediate. The presence of salt products, including CH_3COONa, $NaNO_3$, Na_2SO_4, and NaCl as mentioned in the mechanisms, was effectively eliminated by the washing process. Thus, XRD patterns of ZnO powders are shown in the purified phase devoid of any contaminated peaks. Moreover, the d-spacing calculations, average crystallite size, and the relative intensity ratio of $I_{(002)}/I_{(101)}$ from various zinc precursors are presented in Table 2. The average crystallite size of the ZnO powders was evaluated by the Debye–Scherrer Equation as follows [33],

$$D = \frac{k\lambda}{\beta \cos\theta} \quad (5)$$

where D is the crystallite size, k is the form factor (0.89), λ is the wavelength of Cu Kα radiation (0.154 nm), β is the width evaluated at mid-high of the most intense diffraction peak, and θ is the Bragg angle. The interplanar d-spacing was calculated through Bragg's Law Equation [34] using the major ZnO peak at the 101 plane [35]. The average crystallite size of ZnO powders derived from different zinc salt precursors is approximately 20 nm to 26 nm, varying based on their morphologies. The largest crystallite size of ZnO material using zinc nitrate precursor was associated with the high aggregation of flake-like structure. Meanwhile, the d-spacing calculations of ZnO powder exhibited insignificant changes indicating minimal impact from variations in the precursor used. The relative intensity ratio of the dominant planes at (002) and (101); $I_{(002)}/I_{(101)}$ in the diffraction patterns of zinc oxide was further studied to investigate the prominent rod-like shape in the ZnO structure. However, the relative ratios obtained by ZnO materials using various zinc salt precursors showed similar values, approximately around 0.5 corresponding to the overall morphology of flake and plate-like.

The chemical bonding of ZnO nanopowder with different zinc salt precursors was conducted using an FT-IR spectrophotometer, with recorded spectra in Figure 4 within the range of 400 cm^{-1} to 4000 cm^{-1}. The FT-IR spectra of all samples consistently revealed vibrational modes corresponding to Zn–O bonding at 454 cm^{-1} and 523 cm^{-1} under each condition. Additionally, the predominant peaks at 690 cm^{-1} and 900 cm^{-1} are associated with Zn–OH [36], originating from the physical absorption of water on the ZnO surface. This result confirms the formation of ZnO powder, indicating the bonding of Zn atoms with oxygen atoms. Meanwhile, the evident peak at 3400 cm^{-1} in the FT-IR spectra was identified to O–H stretching from the hydroxyl group [37]. Therefore, all FT-IR spectra of ZnO powder using various zinc precursors reveal the functional groups in ZnO bonding, which correspond to pure ZnO without any chemical contamination in all zinc salt precursors.

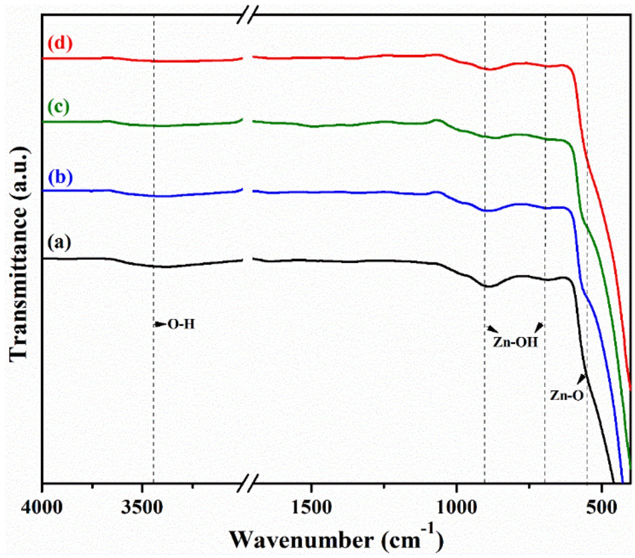

Figure 4. FT-IR spectra of ZnO nanopowders with different zinc precursors of (a) zinc acetate, (b) zinc sulphate, (c) zinc chloride, and (d) zinc nitrate.

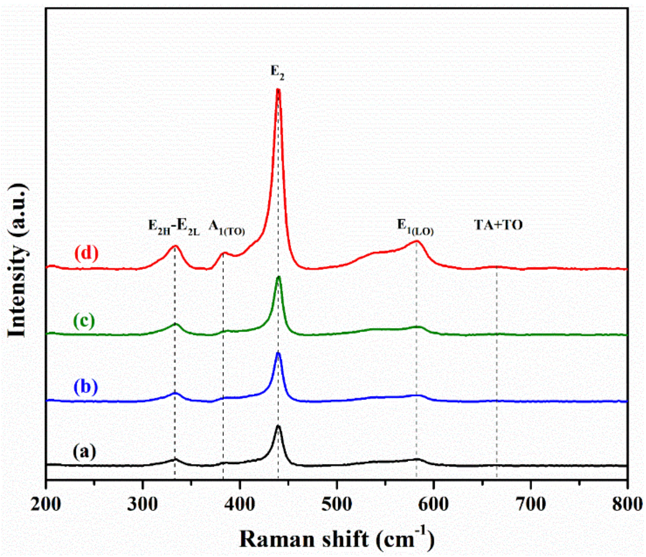

Figure 5. Raman patterns of ZnO nanopowders with different zinc precursors of (a) zinc acetate, (b) zinc sulphate, (c) zinc chloride, and (d) zinc nitrate.

Table 2. d-spacing calculations, average crystallite size and the $I_{(002)}/I_{(101)}$ intensity ratio of ZnO nanopowders with different zinc precursors.

ZnO powder from different precursors	$I_{(002)}/I_{(101)}$	d_{hkl} (Å)	Average crystallitesSize (nm)
Zinc acetate	0.51	2.5918	20.7
Zinc sulphate	0.54	2.5962	21.2
Zinc chloride	0.50	2.5940	21.6
Zinc nitrate	0.53	2.6035	25.3

The Raman spectra acquired from the ZnO nanopowder are depicted in Figure 5. Identical spectra were obtained for all samples using different zinc salt precursors corresponding to FTIR analysis. The observed Raman spectra in the ZnO powder are attributed to the Raman-active vibrational modes of the hexagonal wurtzite ZnO structure, and no impurity-related Raman peaks are evidently in the spectrum. The optical phonons at the zone center, predicted by group theory $A_1 + E_1 + 2E_2$. The modes of A_1 and E_1 symmetry are polar phonons, exhibiting distinct frequencies for the transverse-optical (TO) and longitudinal-optical (LO) phonons. Raman intensity peak in the spectrum of ZnO powder is observed at 440 cm^{-1} of sharp E_{2H} mode, attributed to oxygen vibration incorporated with Zn sublattice [38]. Meanwhile, the observed peaks at 335 cm^{-1} and 590 cm^{-1} were attributed to $E_{2H} - E_{2L}$ and $E_{1(L)}$ mode. The non-activated state of ZnO nanopowder reveals a pronounced second-order Raman mode with A_1 symmetry, particularly notable in the ZnO sample derived from zinc nitrate [29]. Therefore, the Raman and FT-IR results were described as chemical bonding, which was found to match the chemical fingerprint as identified to pure ZnO powder. The highest Raman intensity strongly occurred in the ZnO sample using zinc nitrate precursor owing to the largest crystallite size as proposed in XRD analysis.

Nitrogen adsorption/desorption isotherms and pore size distribution measurements at liquid N_2 temperature 80°C of ZnO nanopowders synthesized using different zinc precursors are presented in Figure 6. The classification based on IUPAC criteria indicates that all the samples exhibited isotherm type IV with H3 type in low altitude distinct hysteresis loop. The results of surface area per volume, cumulative volume, and average pore diameter are presented in Table 3. The average pore diameter of all ZnO nanopowder using different zinc salt precursors is in the range of 6.2 to 7.6 nm corresponding to mesoporous structure with the isotherm type IV [39]. Moreover, H3 type hysteresis loop is not affected by limiting adsorption at high P/P_0 which is typically associated with aggregated particles [40]. The ZnO material exhibiting the highest specific surface area was achieved by a zinc sulfate precursor, attributed to its flat-plate structure. The specific surface area of the ZnO sample using a zinc acetate precursor was similar to that of the sample with a zinc sulfate precursor, due to the mixture of small rod-like and plate-shape ZnO nanostructures. Meanwhile, the lowest specific surface area was observed in the samples using zinc chloride and zinc nitrate, which was related to the high aggregation of ZnO cluster.

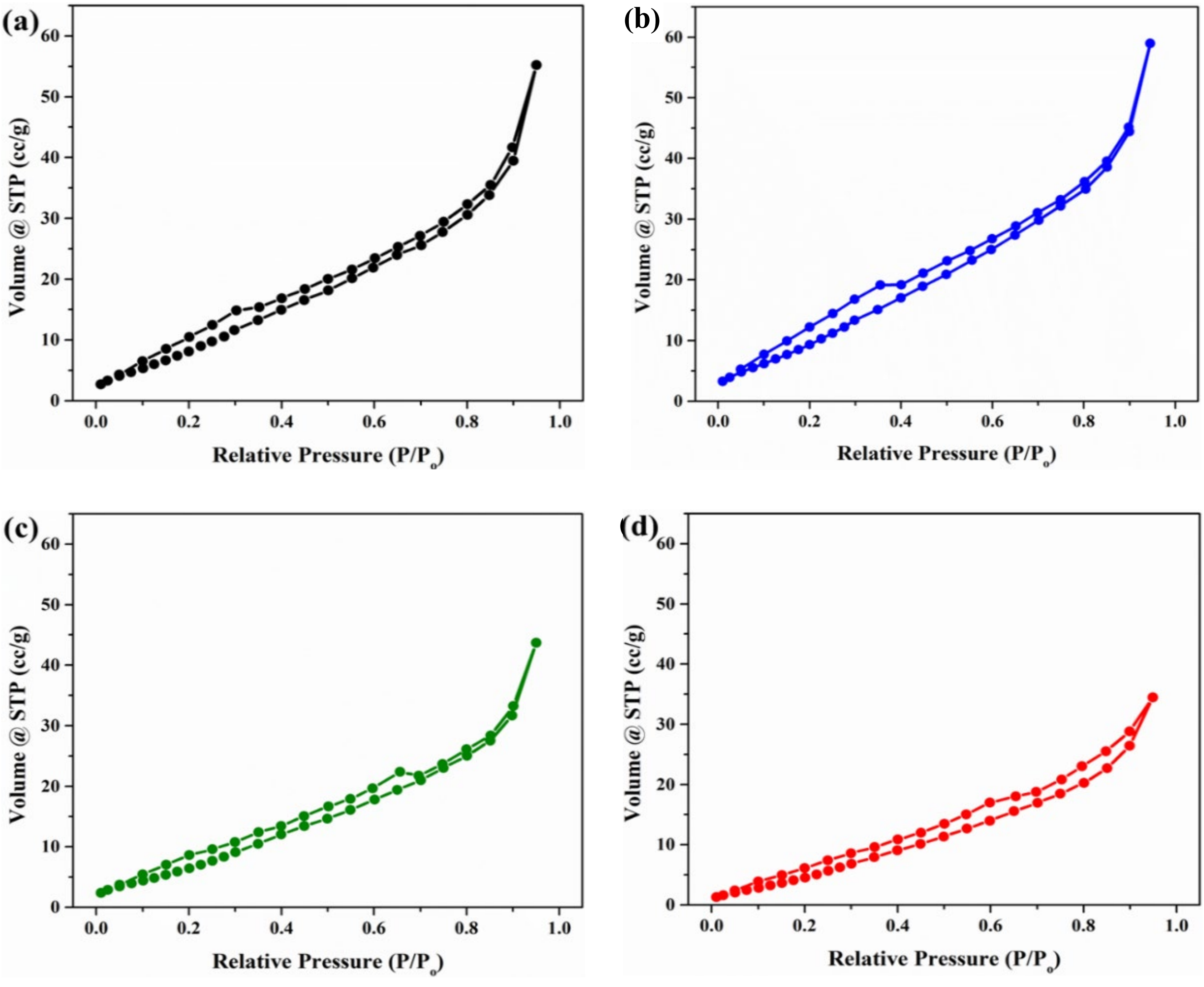

Figure 6. N_2-isotherms of ZnO nanopowders using zinc precursors (a) zinc acetate, (b) zinc sulphate, (c) zinc chloride, and (d) zinc nitrate.

Table 3. Results of surface area per volume, cumulative volume, and average pore diameter.

Samples	BET surface area ($m^2 \cdot g^{-1}$)	Cumulative volume (1–50 nm) ($cm^3 \cdot g^{-1}$)	Average pore diameter (nm)
Zinc acetate	50.29	0.085	6.8
Zinc sulphate	58.38	0.091	6.2
Zinc chloride	35.33	0.067	7.6
Zinc nitrate	30.48	0.053	7.0

4. Conclusions

ZnO nanopowders with different structures were synthesized via a one-step sol-gel process under mild thermal energy. ZnO products synthesized from various zinc salt precursors exhibited a high crystallinity in the ZnO wurtzite structure, devoid of impurities from starting materials and intermediates. Notably, the formation of ZnO from zinc hydroxide intermediate is particularly evident during the synthesis, relating to the purity of ZnO powders obtained from all zinc salt precursors as confirmed by the similar analysis of XRD patterns, FTIR spectra, and Raman characteristics. The structural characteristics of these ZnO structures exhibited small rod-shaped and flake-like structures with distinct formations depending on the types of zinc salt precursors, consequently affecting the resulting different morphology and surface area. The highest specific surface area was observed in the ZnO sample using zinc sulfate precursor owing to the optimized structure in small flake-like. The mixture of small rod-like and plate-shaped ZnO nanostructures observed in the ZnO sample using a zinc acetate precursor exhibited a similar specific surface area to the sample with a zinc sulfate precursor. This finding is interesting for further investigation to enhance the ZnO-specific surface area utilized in the sensing membrane and effective photocatalysts.

Acknowledgements

This work has been supported from the KMITL Research and Innovation Services (KRIS) with the grant No. KREF026702. Meanwhile, the facility and analytical instrument have been greatly obtained by College of Materials Innovation and Technology, King Mongkut's Institute of Technology Ladkrabang (KMITL) and Opto-Electrochemical Sensing Research Team (OEC), National Electronics and Computer Technology Center (NECTEC).

References

[1] A. N. U. Haq, A. Nadhman, I. Ullah, G. Mustafa, M. Yasinzai, and I. Khan, "Synthesis approaches of zinc oxide nanoparticles: the dilemma of ecotoxicity," *Journal of Nanomaterials*, vol. 2017, no. 12, p. 851034, 2017.

[2] S. Majumder, P. Basnet, J. Mukherjee, and S. Chatterjee, "Effect of zinc precursor on morphology of ZnO nanoparticles," *AIP Conference Proceedings*, vol. 2273, no. 1, p. 040006, 2020.

[3] P. K. Aspoukeh, A. A. Barzinjy, and S. M. Hamad, "Synthesis, properties and uses of ZnO nanorods: a mini review," *International Nano Letters*, vol. 12, pp. 153-168, 2021.

[4] A. Ejsmont, and J. Goscianska, "Hydrothermal synthesis of ZnO superstructures with controlled morphology via temperature and pH optimization," *Materials,* vol. 16, p. 1641, 2023.

[5] H. T. T. Thuong, C. T. T. Kim, L. N. Quang, and H. Kosslick, "Highly active brookite TiO_2-assisted photocatalytic degradation of dyes under the simulated solar−UVA radiation," *Progress in Natural Science: Materials International*, vol. 29, pp. 641-647, 2019.

[6] K. Dulta, G. K. Ağçeli, P. Chauhan, R. Jasrotia, and P. K. Chauhan, "Ecofriendly synthesis of zinc oxide nanoparticles by carica papaya leaf extract and their applications," *Journal of Cluster Science*, vol. 33, pp. 603-617, 2021.

[7] R. Rathore, and N. Kaurav, "The structural and optical properties of ZnO nanoparticles synthesized via thermal decomposition," *Materials Today: Proceedings*, vol. 54, pp. 624-627, 2022.

[8] G. Wisz, I. Virt, P. Sagan, P. Potera, and R. Yavorskyi, "Structural, optical and electrical properties of zinc oxide layers produced by pulsed laser deposition method," *Nanoscale Research Letters*, vol. 12, p. 253, 2017.

[9] Y. Bai, J. Zhao, Z. Lv, and K. Lu, "Enhanced piezocatalytic performance of ZnO nanosheet microspheres by enriching the surface oxygen vacancies," *Journal of Materials Science*, vol. 55, pp. 14112-14124, 2020.

[10] S. D. Lokhande, M. B. Awale, and V. D. Mote, "Optical and gas sensing properties of Cu-doped ZnO nanocrystalline thin films for sensor applications," *Journal of Materials Science: Materials in Electronics*, vol. 33, pp. 25063-25077, 2022.

[11] T. U. D. Thi, T. T. Nguyen, Y. D. Thi, K. H. T. Thi, B. T. Phan, and K. N. Pham, "Green synthesis of ZnO nanoparticles using orange fruit peel extract for antibacterial activities," *RSC Advances*, vol. 10, pp. 23899-23907, 2020.

[12] D. R. Hang, K. H. Sharma, C. H. Chen, and S. E. Islam, "Enhanced photocatalytic performance of ZnO nanorods coupled by two-dimensional α-MoO_3 nanoflakes under UV and visible light irradiation" *Chemistry A European Journal,* vol. 22, pp. 1-9, 2016.

[13] J. Jiang, Y. Li, S. Tan, and Z. Huang, "Synthesis of zinc oxide nanotetrapods by a novel fast microemulsion-based hydrothermal method," *Materials Letters*, vol. 64, no. 20 pp. 2191-2193, 2010.

[14] W. Qian, K. Zhao, D. Zhang, C. R. Bowen, Y. Wang, and Y. Yang, "Piezoelectric material-polymer composite porous foam for efficient dye degradation via the piezo-catalytic effect," *ACS Applied Materials & Interfaces*, vol. 11, pp. 27862-27869, 2019.

[15] Y. Chimupala, C. Phromma, S. Yimklan, N. Semakul, and P. Ruankham, "Dye wastewater treatment enabled by piezo-enhanced photocatalysis of single-component ZnO nanoparticles," *RSC Advances*, vol. 10, no. 48, pp. 28567-28575, 2020.

[16] R. Müller, F. Huber, O. Gelme, M. Madel, J. P. Scholz, A. Minkow, U. Herr, and K. Thonke, "Chemical vapor deposition growth of zinc oxide on sapphire with methane: initial crystal

formation process," *Crystal Growth & Design*, vol. 19, no. 9, pp. 4964-4969, 2019.

[17] L. Nafar, R. Rasuli, M. FallahBarzoki, M. Sajadi, and M. Sajadi, "Arc-discharge synthesis of ZnO:Ag nanoparticles for photocatalytic applications: effects of aging, microwave radiation, and voltage," *Plasmonics*, vol. 18, pp. 2305-2314, 2023.

[18] S. K. Lim, S. H. Hwang, S. Kim, and H. Park, "Preparation of ZnO nanorods by microemulsion synthesis and their application as a CO gas sensor," *Sensors and Actuators B: Chemical*, vol. 160, pp. 94-98, 2011.

[19] P. Rattanawarinchai, N. Khemasiri, S. Jessadaluk, C. Chananonnawathorn, M. Horprathum, A. Klamchuen, N. Kayunkid, S. Rahong, D. Phromyothin, and J. Nukeaw, "Growth time dependence on photoelectrochemical property of ZnO nanorods prepared by hydrothermal synthesis," *Surface Review and Letters*, vol. 25, p. 1840001, 2018.

[20] G. Taka, and T. D. Das, "Synthesis of ZnO nanoparticles through a simple wet chemical precipitation method," *IOP Conference Series: Earth and Environmental Science*, vol. 1042, p. 012017, 2022.

[21] P. K. Vabbina, R. Sinha, A. Ahmadivand, M. Karabiyik, B. Gerislioglu, O. Awadallah, and N. Pala, "Sonochemical synthesis of a zinc oxide core–shell nanorod radial p–n homojunction ultraviolet photodetector," *ACS Applied Materials & Interfaces*, vol. 9, pp. 19791-19799, 2017.

[22] J. N. Hasnidawani, H.M. Azlina, H. Norita, N. N. Bonnia, S. Ratim, and E. S. Ali, "Synthesis of ZnO nanostructures using sol-gel method," *Procedia Chemistry*, vol. 19, pp. 211-216, 2016.

[23] C. Aiempanakit, T. Phantaporn, and K. Aiempanakit, "Enhanced photocatalytic activity of ZnO nanostructures deposited on mesh through electrochemical deposition and thermal oxidation," *Journal of Metals, Materials and Minerals*, vol. 32, pp. 63-69, 2022.

[24] S. Abubakar, S. T. Tan, J. Y. C. Liew, Z. A. Talib, R. Sivasubramanian, C. A. Vaithilingam, S. S. Indira, W. C. Oh, R. Siburian, S. Sagadevan, and S. Paiman, "Controlled growth of semiconducting ZnO nanorods for piezoelectric energy harvesting-based nanogenerators," *Nanomaterials*, vol. 13, no. 6, pp. 1052, 2023.

[25] G. Yergaliuly, B. Soltabayev, S. Kalybekkyzy, Z. Bakenov, and A. Mentbayeva, "Effect of thickness and reaction media on properties of ZnO thin flms by SILAR," *Scientific Reports*, vol. 12, no. 851, 2022.

[26] V. V. Pokropivny, and V. V. Skorokhod, "Classification of nanostructures by dimensionality and concept of surface forms engineering in nanomaterial science," *Materials Science and Engineering: C*, vol. 27, pp. 990-993, 2007.

[27] X. Wang, M. Ahmad, and H. Sun, "Three-dimensional ZnO hierarchical nanostructures: solution phase synthesis and applications," *Materials*, vol. 10, no. 11, pp. 1304, 2017.

[28] B. Manikandan, T. Endo, S. Kaneko, K. R. Murali, and R. John, "Properties of sol gel synthesized ZnO nanoparticles," *Journal of Materials Science: Materials in Electronics*, vol. 29, pp. 9474-9485, 2018.

[29] S. Al-lami, and H. Jaber, "Controlling ZnO nanostructure morphology on seedless substrate by tuning process parameters and additives," *Chemistry and Materials Research*, vol. 6, no. 4, pp. 101-109, 2014.

[30] M. A. Gatou, N. Lagopati, I. A. Vagena, M. Gazouli, and E. A. Pavlatou, "ZnO nanoparticles from different precursors and their photocatalytic potential for biomedical use," *Nanomaterials*, vol. 13, pp. 122, 2023.

[31] J. A. A. Abdullah, A. Guerrero, and A. Romero, "Efficient and sustainable synthesis of zinc salt-dependent polycrystal zinc oxide nanoparticles: comprehensive assessment of physicochemical and functional properties," *Applied Sciences*, vol. 14, pp. 1815, 2024.

[32] C. C. Lin, and Y. C. You, "Mass-production of ZnO nanoparticles by precipitation in a rotating packed bed: effect of zinc salt," *Journal of Materials Research and Technology*, vol. 9, pp. 8451-8458, 2020.

[33] S. Mustapha, M. M. Ndamitso, A. S. Abdulkareem, J. O. Tijani, D. T. Shuaib, A. K. Mohammed, and A. Sumaila, "Comparative study of crystallite size using Williamson-Hall and Debye-Scherrer plots for ZnO nanoparticles," *Advances in Natural Sciences: Nanoscience and Nanotechnology*, vol. 10, pp. 045013, 2019.

[34] A. K. Arora, S. Devi, V. S. Jaswal, J. Singh, M. Kinger, and V. D. Gupta, "Synthesis and characterization of ZnO nanoparticles," *Oriental Journal of Chemistry*, vol. 30, no.4, pp. 1671-1679, 2014.

[35] V. Kumar, H. C. Swart, O. M. Ntwaeaborwa, R. E. Kroon, J. J. Terblans, S. K. K. Shaat, A. Yousif, and M. M. Duvenhage, "Origin of the red emission in zinc oxide nanophosphors," *Materials Letters*, vol. 101, pp. 57-60, 2013.

[36] A. Taufiq, H. N. Ulya, J. Utomo, Sunaryono, N. Hidayat, H. Susanto, N. Mufti, Munasir, and S. Soontaranon, "Structural, optical, and antifungal characters of zinc oxide nanoparticles prepared by sol-gel method," *Journal of Physics: Conference Series*, vol. 1093, p. 012001, 2018.

[37] M. Aiempanakit, P. Sudjai, K. Singsumphan, S. Laksee, and C. Suwanchawalit, "Brazilein modified zinc oxide nanorods with enhanced visible light-responsive photocatalytic efficiency," *Journal of Metals, Materials and Minerals*, vol. 32, pp. 70-76, 2022.

[38] Q. Huang, and J. Liu, "Facile and clean solution synthesis of large-scale ZnO nanorods assisted with aliquat 336," *Journal of Chemistry*, vol. 2013, pp. 1-6, 2013.

[39] Z. Jowkar, A. Moaddeli, F. Shafiei, T. Tadayon, and S. A. Hamidi, "Synthesis and characterization of mesoporous zinc oxide nanoparticles and evaluation of their biocompatibility in L929 fibroblasts," *Clinical and Experimental Dental Research*, vol. 10, p. e844, 2024.

[40] U. Pal, C. W. Kim, N. A. Jadhav, and Y. S. Kang, "Ultrasound-assisted synthesis of mesoporous ZnO nanostructures of different porosities," *The Journal of Physical Chemistry C*, vol. 113, pp. 14676-14680, 2009.